Combustion Science and Technology

ISSN: (Print) (Online) Journal homepage: https://www.tandfonline.com/loi/gcst20

Experiments, Modeling and Correlation for Smoldering of Incense Sticks

H. S. Mukunda, A. Shivakumar, Sachin Payyanad, A.Ve. Sowriraajan & C.S. Bhaskar Dixit

To cite this article: H. S. Mukunda, A. Shivakumar, Sachin Payyanad, A.Ve. Sowriraajan & C.S. Bhaskar Dixit (03 Dec 2023): Experiments, Modeling and Correlation for Smoldering of Incense Sticks, Combustion Science and Technology, DOI: 10.1080/00102202.2023.2288207

To link to this article: https://doi.org/10.1080/00102202.2023.2288207

COMBUSTION SCIENCE AND TECHNOLOGY
https://doi.org/10.1080/00102202.2023.2288207

Taylor & Francis
Taylor & Francis Group

Experiments, Modeling and Correlation for Smoldering of Incense Sticks

H. S. Mukunda, A. Shivakumar, Sachin Payyanad, A.Ve. Sowriraajan, and C.S. Bhaskar Dixit

Fire & Combustion Research Center, Jain (Deemed-to-be) University, Bangalore, Karnataka, India

ABSTRACT

This paper is concerned with the modeling of smoldering characteristics of incense sticks under free convection. Experimental data on smoldering characteristics are presented on specifically designed compositions from biomass to char, involving measurements of smoldering rate, condensed phase temperature with time and hence the distance and shape of the steadily smoldering surface. The modeling effort invokes a steady surface heat balance, expressing it in dimensionless terms and relating the smoldering Reynolds number, Re_r, to the heat transfer by convection through transfer number, B, Grashof number, Gr, and flow Reynolds number, Re_v. Three constants in the model are determined by seeking to minimize the differences with the experimental data. The extinction criterion that emerges from the data analysis is expressed in terms of smoldering Reynolds number. The shape of the smoldering front is shown to be related to the stoichiometric ratio that varies from biomass to char. While the predictions are shown to be good in most cases, the lack of experimental details in select cases is argued as the cause of lack of better comparison. A correlation of the smoldering Reynolds number in terms of transfer number B that depends on compositional parameters, oxygen fraction and ambient pressure is shown to predict the smoldering rate to within ±7% as well as extinction.

ARTICLE HISTORY
Received 24 July 2023
Revised 3 November 2023
Accepted 22 November 2023

KEYWORDS
Smoldering rate; modeling; correlation; incense sticks

Introduction

Smoldering phenomenon is observed in several applications. Incense sticks used in religious functions and also those with supposed health benefits have been pursued in the east for a long time. Cigarette combustion process is another smoldering phenomenon that has been studied because of the possibility of it being a fire risk when handled carelessly in domestic environment (Baker 1977). Transition from smoldering to flaming when left on fabrics in sitting places is the reason for serious concern. Many other applications have been examined by Rein (2009), who emphasized the need for a greater degree of scientific attention, and in their paper, Torero et al. (2020) have attempted to provide a wide-ranging view of smoldering more generally in a packed bed mode.

Moussa, Toong, and Garris (1977) conducted an important early study on the smoldering of cotton strands (0.5–8 *mm*) in view of fire safety considerations. The thesis by Moussa (1976) has provided an approximate description of the physical processes, namely, pyrolysis

CONTACT A. Shivakumar shivakumar.a@jainuniversity.ac.in Fire & Combustion Research Center, Jain (Deemed-to-be) University, Kanakapura Road, Bangalore, Karnataka, India
Supplemental data for this article can be accessed online at https://doi.org/10.1080/00102202.2023.2288207

in which volatiles come off the pre-char zone and the char-oxygen reaction that maintains the char zone at high temperature, with the latter diffusing from the surroundings. The experiments were conducted with very low density materials (60 kg/m^3) largely in a horizontal mode with the fuel elements spread over a fine metal mesh at different pressures including sub-atmospheric conditions and oxygen fractions. The results showed smoldering rates of 13–23 mm/min with surface temperature varying between 1000 K and 1200 K. They evaluate the product of ρ_f, $\dot{r}$ and d, seeking greater scaling ability for the parameter. The division by a μ_g (or for that matter, k_s/c_{pg}) would lead to a dimensionless parameter like a Reynolds number, $\rho_f \dot{r} d/\mu_g$.

Moussa, Toong, and Garris (1977) indicate clearly that the smoldering process is diffusion limited, and yet they present a complex surface kinetics supported one-dimensional model to predict the smoldering behavior. The kinetic parameters have such high activation energy that any small change in the surface temperature causes a significant change in the smoldering rate. However, the measured data of smoldering rate show a very weak dependence on the surface temperature, indicating that the apparent activation energy is small.

Mukunda et al. (2007) studied the forward and reverse smoldering of commercially sourced incense sticks (3–10 mm) as a function of stream speed and oxygen fraction in the stream. They also developed a dimensionless scaled model based on a smoldering Reynolds number to explain the behavior in forward and reverse smolder and compared the results with the experiments. They developed the correlations using dependence on Reynolds number and Grashof number along the lines of the well-known Ranz and Marshall correlation (Ranz and Marshall 1952).

Yamazaki, Matsouka, and Nakamura (2018, 2019) have conducted experimental studies on commercial incense sticks at different oxygen mass fractions and ambient pressures. At larger mass fractions of oxygen, the smoldering mode is limited to lower pressures and below a certain pressure extinction occurs.

Lin, Chow, and Huang (2021) conducted studies on incense sticks akin to Mukunda et al. (2007), exploring the effects of diameter (1.5, 2.5 and 5.0 mm) and density 720, 920 and 1,100 kg/m^3. The values of density appear to be nominally identified since there seems no variation of the value across the samples used in various experiments. The fact that this can be an issue is seen from an earlier work by Momeni et al. (2012) on the combustion of biomass spheres and cylinders, where they indicate a density of 600 kg/m^3 in the text, but the values of density computed from the data of dimensions and mass provided by them lead to 840, 540 and 577 kg/m^3 for different samples. Hence, it is important to evaluate the density for individual samples to preserve the integrity of the data, more particularly if the details of geometry and mass are not reported. They present several scaling arguments ignoring the earlier work on modeling in Mukunda et al. (2007) and have not brought their arguments up to the stage of predictive capability. Chirag et al. (2011) studied the smoldering of teak wood and cow dung and reported their experimental results.

Yan et al. (2022) have studied the smoldering of char cones made of cyprus and elm barks of 2–7 mm diameter and with large ash content and presented the data on the smoldering rate, the surface temperature, the relationship between heights of char cone and the carbon consumption rate. The last result has been set out as consistent with the gas phase diffusion flame behavior. They have provided the details of the composition, enabling the possibility of comparisons with the predictions in the present study.

Sowriraajan et al. (2023) determined the smoldering rate of a number of specifically designed compositions around those deployed in incense stick manufacturing industry to uncover the reasons for low-probability self-extinction of smoldering incense sticks and provide data for modeling the behavior as a function of the composition. This investigation ruled out the role of phosphorous compounds and silica even at reasonably large fractions and homed on to the presence of termite-infested mud. Specifically, antigorite, a compound found in termite mud, decomposes endothermically at temperatures close to the surface temperature of the smoldering incense stick and reduces the surface temperature to low values leading to extinction.

In view of the above literature, it seems important to recognize the fact that the smoldering behavior is affected by the diameter, density and the composition of the incense sticks with a factor of 2 variation of linear smoldering rates and also with a burn flux. Furthermore, it is also understood that the smoldering experiments are largely performed on the commercially available incense sticks without the knowledge of the composition of the ingredients in the incense stick. Also, in some cases, the nominal density values are reported without actual densities of the individual sticks. On the modeling side, the earlier work in Mukunda et al. (2007) had explored largely the forced convective effects, but inadequately explored the smoldering under free convective conditions, particularly, the role of individual components.

In the present work, the smoldering experiments of incense sticks are performed for a wide range of compositions by varying the composition from 100% biomass to nearly 100% charcoal and also determine their effects on the formation of the char cone. In the modeling part, a correlation has been deduced to account for the effect of incense stick composition and externally imposed variations of oxygen fraction and pressure on the smoldering behavior. The focus of the latter effort is to use physics-based modeling, bringing together as much of measured data as possible, both from earlier literature and the experiments conducted here to predict the burn flux of the incense sticks. Also, the attempt is to obtain additional information on the cone height-to-diameter ratio for the variety of compositions and explain the behavior.

Present experiments and observations

The incense stick is made up of various components largely having biomass and char in powder form. In addition, ingredients like jigit (powdered dry bark of the *Litsea glutinosa* tree) are used as a binder and, of course, an aromatic chemical liquid is used to obtain aroma from the evaporation of the chemical. On occasion, guar gum is also used as a binding agent. In some instances, potassium nitrate is added as a smolder rate enhancer. While these are the expected components in a normal composition, it may turn out that inorganics like sand and termite mud sticking to the bark may enter into the composition inadvertently. In view of this, it was decided to make incense sticks with known compositions containing various ingredients.

Experimental methods

To perform the smoldering experiments, the incense sticks were produced in-house by obtaining the most raw ingredients, namely, biomass powder, char powder, jigit (a natural

adhesive) and guar gum from a manufacturing industry. Furthermore, a select set of normally smoldering incense sticks and a set that was extinguishing after the initial smoldering were procured. The ash fraction is the mass fraction of the material left after subjecting the sample to a temperature of 650 ± 20°C in a muffle furnace for 3 hours. The ash fraction of the procured raw samples of char, biomass and jigit are 25.3%, 8.6% and 4%, respectively.

To produce the incense sticks of diameters 3–8 *mm* of various compositions, the raw materials for the select compositions were introduced into a high speed mixer and the entire mixture underwent both size reduction and intimate mixing. Then, it was mixed with about 35% water and extruded in a handheld screw press to get the wet incense sticks. After that, they were placed in an oven at 100°C to get the dried incense sticks and then were allowed to cool down to ambient temperature, before the dimensions and mass were measured. A total of 50 different compositions were prepared, and the various fractions used in making the incense sticks are denoted by f_b for biomass (with jigit and/or guar gum treated as biomass), f_c for char, f_w for moisture and f_{ash} for ash (the final residue). In a few cases, specific ingredients like silicon dioxide were also added to explore the effects on smoldering behavior.

A brief segment of the full table set is presented in Table 1 to aid understanding. Compositions 1, 8, 13, 19, 20 and 27 relate to 100% biomass to 95% carbon.

The full set of data on the compositions appears in Appendix (Tables A1 and A2). Compositions 1–3 are of biomass only. In these tables, compositions 4–7 have a 20% introduction of char into the sample extruded at a range of diameters up to 8 *mm*. Detailed compositions vary around this value. Composition 8 has roughly equal proportions of char and biomass. Compositions 9–12 are produced by the deliberate introduction of fine silica sand in different proportions from 5% to 20% into largely char; the small amount of biomass from Jigit is used as a binding agent. The varying silica fractions get reflected in a much larger fraction of ash in these cases. Compositions 13–20 are produced around 80–95% char. Composition 21, termed CG, is the sample incense stick from the industry. Samples 22–24 were made by introducing 16% jigit and 18% guar gum in biomass. Compositions 25–27 are the same as in the study (Sowriraajan et al. 2023), and these contain sand at 17% and 31% of the solids and termite mud at 29% of the solids.

Table A2 contains compositions 28–33 that are similar to those produced in the industry and compositions 34–37 that are from an earlier work (Mukunda et al. 2007). Among all these compositions, only composition 27 containing termite mud extinguished.

Table 1. Composition and basic data of incense sticks and measured smoldering data and calculated parameters for the correlation on smoldering rate, $Y_{ox} = 0.232$, ambient pressure, $p_a = 95$ kPa, B = biomass, C = char, ga-M = guar gum, rat = ratio of CO to CO_2.

No.	Type	f_b	f_c	f_w	f_{ash}	f_{eff}	ρ_f kg/m³	d mm	r mm/min	$\rho_f r$ g/m²s	h/d
1	100 B,1	0.751	0	0.092	0.157	0.225	778	2.9	3.31	43.5	1.38
8	55B, 45C	0.710	0.123	0.103	0.064	0.336	885	3.2	3.00	44.3	1.72
9	20SiO2-C	0.035	0.520	0.036	0.271	0.530	864	6.2	2.20	31.7	3.24
13	80C, 20B	0.158	0.628	0.040	0.174	0.676	730	8.5	2.50	30.4	
19	90C, 10B	0.079	0.708	0.041	0.171	0.732	725	6.6	2.97	35.9	3.80
20	95C, 5B	0.039	0.747	0.042	0.171	0.759	735	6.2	3.05	37.4	4.05
27	C-3-Te-M	0.272	0.223	0.037	0.266	0.305	800	8.5	Ext	Ext	

In these tables, a quantity, namely, effective fraction undergoing smoldering, f_{eff}, is introduced. It is the sum of char fraction and a part left behind as char after the volatiles are released from the biomass. Experiments performed here by introducing with bamboo stick and biomass separately into a coarse sand bed kept at 300°C and 350°C showed values of 26.5% and 28 for bamboo and 32% and 36.7% for wood powder obtained from the industry. It should be noted that the wood powder has 8–9% ash. In view of these features, a mean value of 30% has been chosen as the value for biomass conversion to char. Therefore, the effective fraction undergoing smoldering is set out as

$$f_{eff} = f_c + 0.3 f_b \tag{1}$$

In the above equation, f_c and f_b are the fractions of char and biomass. The reason for invoking f_{eff} is that the material that undergoes smoldering is inferred to be char that is left behind after pyrolysis is described in section 2.2.

Once the sticks of required composition are prepared, markings are made on the sticks at a distance of 5 *mm* for a length of about 8–10 *cm*, mounted vertically and lit at the top as shown in Figure 1, the stick is allowed to smolder for about 25–30 *mm* to reach steady smoldering and then the time required for the smoldering front to reach each marking was recorded from which the smoldering rate was determined. Each experiments were repeated three times to check the repeatability. In select experiments, condensed phase temperature–

Figure 1. Photograph of a smoldering incense stick with volatiles issuing from all around below the red hot zone.

time curve is obtained in order to extract the information on the heat drawn into the solid during smoldering. For this purpose, K-type thermocouples of 100 micron bead diameter were introduced into 0.3 *mm* holes drilled across the diameter at two locations 5 *mm* apart and in few samples three thermocouples are used, each placed 5 *mm* apart. The spacing was chosen so that the entire thermal profile that may be about 5–8 *mm* deep inside the solid would be extracted after the steady smoldering was achieved.

Experimental results

Figure 1 shows the photograph of a smoldering incense stick. When this photograph is carefully observed, it becomes evident that the volatiles are issuing out of the stick distinctly below the hot smoldering zone (by about a few *mm*). The reason for this is inferred as follows. It is first recognized that the surface temperature of the smoldering zone is about 1000 *K* from references (Lin, Chow, and Huang 2021; Moussa 1976; Moussa, Toong, and Garris 1977; Yamazaki, Matsouka, and Nakamura 2018) as well as from the data obtained in the present study. Under steady smoldering conditions, conduction into the solid maintains temperature profile described in Yamazaki, Matsouka, and Nakamura (2018) and also set out later in this paper. The profile transitions through 650 *K*, which is the range of temperatures for the release of moisture, aromatic components and the products of degradation from biomass (see for instance Mukunda 2011). Therefore, what undergoes fuel–oxidant reaction is limited to the char segment of the incense material. There is another collateral evidence in favor of the above inference. Studies on biomass sphere combustion (Varunkumar, Rajan and Mukunda 2011) have shown that the transition from biomass to char takes place beginning from 600 *K* with flaming around the sphere and the smoldering of char begins at around 1000 *K* and continues till complete conversion. In the case of incense sticks, the surface attains 1000 *K* almost immediately and maintains at that *because the volatiles escape from the side without having to go through the hot layer (if it gets processed by the hot surface, one can no longer get the aromatic smelling volatiles).*

Therefore, smoldering occurs with the char in the presence of inert fraction of the incense stick. The magnitude of char from biomass under oxidative degradation is about 28–32%. In the present study it is taken as 30%. Thus, the material that undergoes oxidative pyrolysis (pyrolysis that occurs in the presence of oxygen as opposed to pyrolysis that occurs in the complete exclusion of oxidizer) is taken to be the sum of 30% of the biomass content of the incense stick and char excluding the inerts.

The data from experiments at our laboratory and those extracted from earlier work (Lin, Chow, and Huang 2021; Moussa 1976; Yamazaki, Matsouka, and Nakamura 2018) are set out as follows:

- Tables A1 and A2 present the compositions in twenty seven and six of the experiments covering the most important features.
- Tables A3 and A4 contain the calculated parameters for the compositions set out in Tables A1 and A2.
- Table A5 contains the data extracted from the experiments of Yamazaki, Matsouka, and Nakamura (2018). Since the data are extensive, only a few of the data are set out.
- Table A6 contains the select data from Moussa (1976).
- Table A7 contains the select data from Lin, Chow, and Huang (2021)
- Table A8 contains the select data from Yan et al. (2022).

Apart from the details of the compositions as discussed earlier, these tables also present the data on the measured values of diameter, density, and the smoldering rate; the mass flux calculated as the product of density and smoldering rate; and the ratio of the height of the cone to the diameter. If we observe the data of Table A1, the following inferences can be drawn: a) with the increase in the diameter of the sample, the smoldering rate reduces (see samples 13, 14 and 15), which is inline with the observations of Lin, Chow, and Huang (2021); b) with the increase in the percentage of inert in the incense, both smoldering and height of the char cone reduce (see samples 9–12), and c) height of the char cone is higher for the samples made with char than the samples made with 100% biomass.

In order to obtain a broad idea of the range of parameters involved, the data are set out in Figure 2. The practical range of ρ_f is about 600–1100 kg/m^3, stick diameters, 2.5–3.5 mm, the mass flux, 20–50 g/m^2s (deduced using the measured smoldering rate $\dot{r}$), and the smolder Reynolds number, 5–20. Experiments made at our laboratory and those of other researchers have covered a wider range. For instance, one extreme is that used in the experiments of Moussa, Toong, and Garris (1977) with the density of cotton at 60 kg/m^3.

Figure 3 shows the plot of the surface temperature with time for 80% biomass and 80% char cases. The temperature profiles show indication to a traveling thermal front, similar to that set out by Yamazaki, Matsouka, and Nakamura (2018). The temperature profiles look similar, albeit with a time shift; this time shift related to the arrival of the smoldering front at these locations. The fact that the speed of propagation is 3.1 mm/min implies that the time taken to arrive is $(5/3.1) \times 60 = 97$ s. If we examine the rising temperature profile (T1), it takes 250 s (from 20 s to 270 s in the case of 80% char, T1). It must be recognized that this time is composed of transient conduction and a uniform propagation of the smoldering

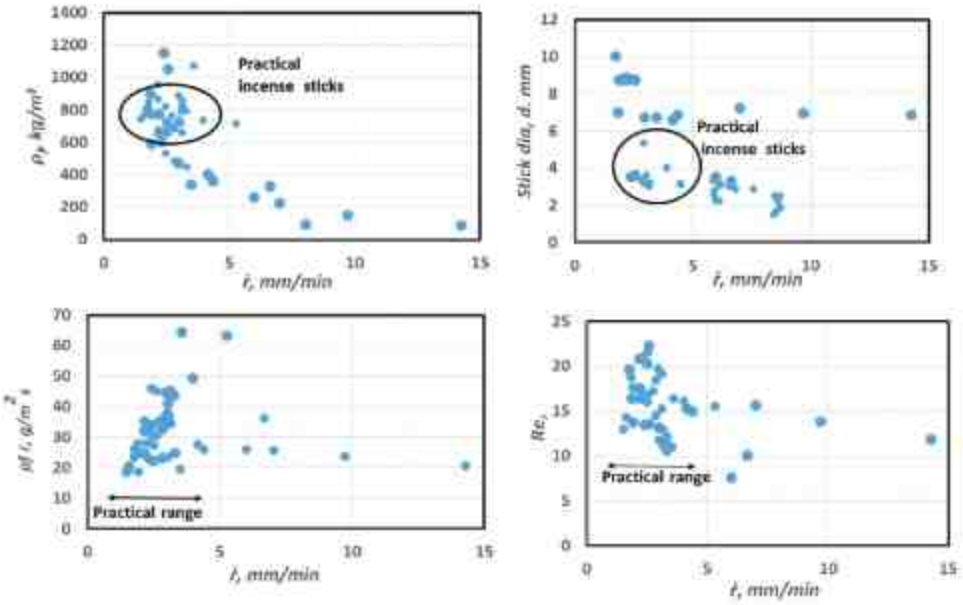

Figure 2. A composite plot of the range of parameters. The abscissa in the plots is the smoulder rate, $\dot{r}$. Top left is the density of the sticks, top right is the diameter of the sticks, bottom left is the smoulder mass flux, $\rho_f \dot{r}$, and bottom right is the smoulder reynolds number, Re_r.

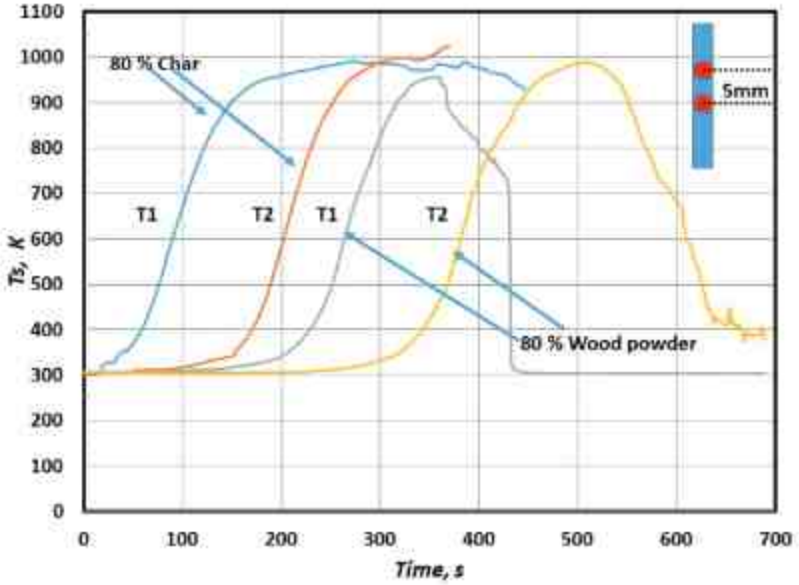

Figure 3. Surface temperature with time for two cases – 80% biomass + 20% char and 80% char + 20% biomass cases, both smoldering at 3.1 ± 0.05 *mm/min* (inscribe is the schematic indicating measurements of T1 and T2, which are 5 *mm* apart).

front. Since the propagation time is 97 s, the transient conduction time, t_{con}, is 153 s (250–97). The transient conduction time in this case is represented by $t_c \sim \alpha_f / \dot{r}^2$. This will provide an estimate of $\alpha_f \sim t_c \dot{r}^2 = 153 \times (3.1/60)^2 = 0.41$ mm^2/s. This can be taken to be an approximate value of the thermal diffusivity under the actual conditions of smoldering. Data from several experiments can be put together on the same coordinate system if we recognize that the temperature profile has translational invariance. Shifting the origins bring together the plots as set out in the left-hand side of Figure 4. An important point to notice is that the temperature profile shows constancy at the peak temperature over some distance of up to 5 *mm*. This zone is covered by ash. Consequently, it can be inferred that radiation loss is insignificant and the loose ash layer acts as a thermal blanket. The lower part of the temperature profile (up to say 650 K) can be understood to be dominated by conduction. The solution to the thermal conduction problem below the surface can be written as

$$(T_s - T)/(T_s - T_0) = exp(-\dot{r}y/\alpha) \tag{2}$$

where $y = 0$ refers to the surface and $y \to \infty$ refers to ambient condition. The surface is regressing at a rate $\dot{r}$. Thus, y can be replaced by $\dot{r}t$. We can express the relationship as

$$ln[(T_s - T_0)/(T_s - T)] = \dot{r}^2 t/\alpha \tag{3}$$

The right-hand side of the plot in Figure 4 shows the data of one composition discussed also in Figure 3 of $ln[(T_s - T_0)/(T_s - T)]$ with time, t. The slope of the curve in the conduction zone is 0.0125 s^{-1}. With $\dot{r} = 0.053$ mm/s, we get α as 0.22 mm^2/s. While the previous value of 0.4 mm^2/s was a simple minded estimate, the presently obtained value is a justifiable value for α, the thermal diffusivity.

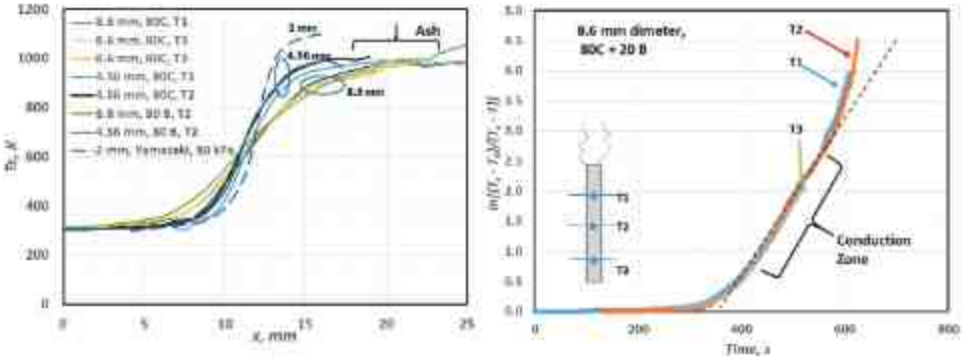

Figure 4. Surface temperature with distance for several compositions with diameters 4.56, 8.60 and 8.80 *mm* smoldering at 3.15 ± 0.05 *mm/min* and the experiment of Yamazaki, Matsouka, and Nakamura (2018) smoldering at 4.73 *mm/min* with wood powder strand of 2 *mm* diameter (left) and scaled dimensionless surface temperature with time emphasizing the conduction zone (right).

With the data presented above, one should be able to construct a physically meaningful model for the smoldering of the incense sticks.

The basic model for smoldering

Figure 5 shows the evolution of the model from the physical behavior of the smoldering stick. The reaction region that has usually a conical shape is shallow (h/d small) for biomass, but high (h/d large) for char. Oxidizer (oxygen in oxygen + nitrogen mixture) diffuses onto the surface and exothermic reaction occurs. It is about 1.5 mm in size. In cases where the ash layer continues to stay over the smoldering front, the ash layer itself forms an insulation and provides for an adiabatic condition. If the ash layer drops off, the temperature drops beyond that. The reaction surface is immediately covered by the ash layer and helps maintain the measured surface temperature. This behavior is also seen in Yamazaki, Matsouka, and Nakamura (2018). The conceptual setting for the mathematical model is set out in Figure 5(c). Below the thin reaction zone lies the char which is 5–7 mm thick. Through this zone, the temperature drops to near ambient temperature of 300 K. In this zone, the biomass degrades to char and the aromatic compounds volatilize and are transported by free convection as smoke.

The overall energy balance can, therefore, be put down as a heat balance equation at the surface of the smoldering front, assuming it to be thin as

$$\dot{q}_c'' = \dot{q}_s'' \tag{4}$$

where $\dot{q}_c''$ is the heat flux into the raw stick, $\dot{q}_s''$ is the heat flux generated by the surface oxidation process, and there is no heat loss term in the equation because of near adiabatic temperature variation beyond the reaction zone. A loose char layer getting settled above the smolder front is the primary reason. This creates adiabaticity. Furthermore, even if the larger ash layer gets dropped, the formation of ash immediately after oxidation maintains a reduced radiation environment for heat loss (section 6.2 in Varunkumar, Rajan, and Mukunda 2013).

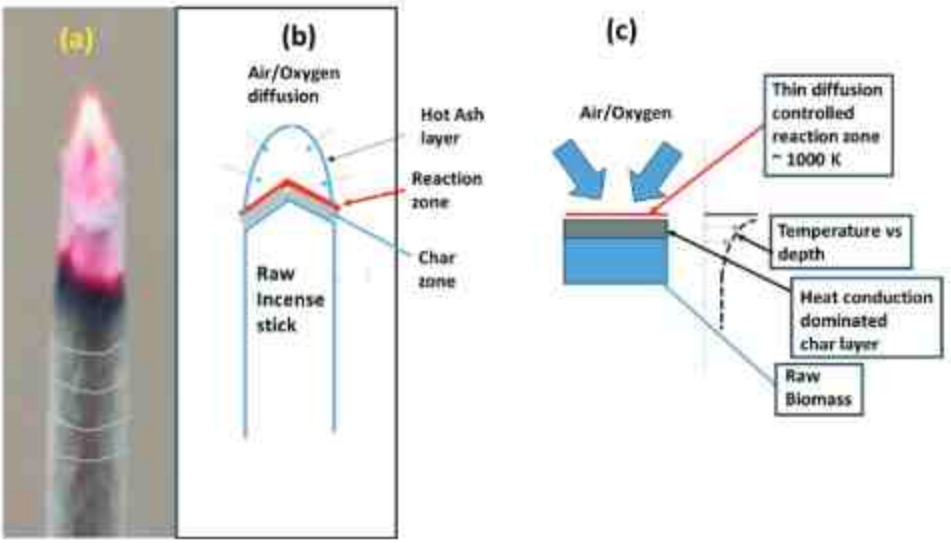

Figure 5. Evolution of the model: (a) smoldering incense stick, (b) cross section showing the principal zones and (c) elements of the model related to the smoldering behavior.

Heat absorption

In this simple model, the condensed heat absorption is expressed as

$$\dot{q}_c'' = \rho_f \dot{r} c_{pf} (T_s - T_0) \tag{5}$$

The value of density, ρ_f, is the one measured for the fuel sample. Value of c_{pf} which is a function of temperature is reported by Dupont et al. (2014) for a number of species. The values vary from 1.3 kJ/kgK to 1.8 kJ/kgK over a temperature range up to 350 K with an increasing trend. In view of the fact that the temperature range is much higher, a single mean value of 1.5 kJ/kgK over the temperature range is chosen. This value is also consistent with that indicated in Ragland, Aerts, and Baker (1991).

Surface heat release

The heat flux generated due to the surface reaction between oxygen that is diffusing onto the surface of the char. The flux, $\dot{q}_s''$, is taken to be proportional to the heat generated at the surface and the mass flux of the oxidizer due to free convection, which is always part of the process and by forced convection when there is flow of the oxidant (air or oxygen–nitrogen mixtures as in some experimental studies). This is set out as

$$\dot{q}_s'' = H_s D\rho \frac{dY_{ox}}{dy} = \frac{H_s}{d} D\rho \frac{dY_{ox}}{d(y/d)} \tag{6}$$

Following the ideas described in Mukunda et al. (2007), this can be recast as

$$\dot{q}_s'' = \frac{H_s}{d} D\rho Y_{ox} f(Gr, Re_u) \tag{7}$$

where $f(Gr, Re_u)$ represents the Nusselt number as a function of Grashof number for natural convection and flow Reynolds number for forced convection. Both these numbers have the usual definition as follows:

$$Gr = \frac{g(1 - T_0/T_s)d^3}{(\mu_g/\rho)^2} \quad \text{and} \quad Re_u = \frac{\rho U d}{\mu} \tag{8}$$

The function $f(Gr, Re_u)$ is taken as

$$f(Gr, Re_u) = C_0(1 + C_1 Gr^{1/4})(1 + C_2 Re_u^{1/2}) \tag{9}$$

The choice of the above expression for convective effects is similar to the ideas of Ranz and Marshall (1952) and those adopted in Mukunda et al. (2007). The expression for $\dot{q}_s''$ becomes

$$\dot{q}_s'' = \frac{H_s}{d} D\rho Y_{ox} C_0 \left(1 + C_1 Gr^{1/4}\right)\left(1 + C_2 Re_u^{1/2}\right) \tag{10}$$

The constants C_0, C_1 and C_2 turn out to be 1, 1 and 0.1 (more discussion on this aspect is done in section 4). Now, the method of determining H_s is discussed. This needs the determination of the oxidation of char that leads to a combination of CO and CO_2 as the gaseous products. The CO/CO_2 ratio affects heat release, since the heat release with CO_2 is 3.5 times that with CO as the product. Several earlier studies on the dependence of CO/CO_2 ratio on temperature and pressure exist. Liu and He (2015) have set out their result as

$$p_{CO}/p_{CO2} = 47 p_{O2}^{-0.23} e^{-3065/T_s} \tag{11}$$

where p_{O2} is the partial pressure of oxygen in atm. The value 3065 K is the activation temperature. Peterson and Brown (2020) have indicated that at temperatures of 500C to 566C, chemical kinetics is sufficiently fast and hence the rate is determined by the external mass transfer rate. The activation temperature deduced by them for pyrolysis rate shows a strong dependence on the material (douglas fir, pine, red oak, willow, switch grass and corn stover) and varies from 1000 K to 3500 K. Mukunda et al. (2007) determined the activation temperature using the data on incense sticks as 5000 K. In view of these differences, the present study uses the following expression:

$$C_{00} = Y_{CO}/Y_{CO_2} = 0.75 \exp[-5000(1/1000 - 1/T_s)] \tag{12}$$

We recognize that the heat of combustion of char to CO and CO_2 are 9.2 and 32.8 MJ/kg. Hence, we can express the heat released at the surface depending on the ratio of CO to CO_2, C_{00} as

$$H_s(\text{MJ/kg}) = f_{eff} \frac{9.2C_{00} + 32.8}{1 + C_{00}} \tag{13}$$

where the right-hand side carries f_{eff} as the coefficient because this is the char fraction that reacts with transported oxygen to cause heat release. We need to add a term related to energy absorption at the surface because of decomposition of ingredients like antigorite and α-quartz, as found in the studies of Sowriraajan et al. (2023). This leads to

$$H_s(\text{MJ/kg}) = f_{eff} \frac{9.2C_{00} + 32.8}{1 + C_{00}} - H_u \tag{14}$$

where H_a is the heat absorbed due to endothermic decomposition at temperatures near the surface temperature of a smoldering incense stick. If potassium nitrate (KNO_3) is added to the composition as is a practice with some manufacturers, it will result in additional exothermic reaction with charcoal. In this case H_a will be negative.

The transfer number, B, and the stoichiometric ratio of oxidation are defined by

$$B = \frac{H_s Y_{ox}}{c_{pf}(T_s - T_0)} \tag{15}$$

$$S = \frac{f_{eff}}{Y_{ox}} \frac{32}{12.1} \tag{16}$$

Transfer number, B, is the ratio of heat release to condensed phase sensible enthalpy with the heat release provided by the exothermic surface reaction in the present case. The stoichiometric ratio, S, is the oxidizer-to-fuel ratio for complete combustion. The term, f_{eff}, is the effective carbon fraction in the sample. For carbon for which $f_{eff} = 1$, at $Y_{ox} = 1$, we get $S = 2.64$. For biomass with 1% ash, S with oxygen will be about 1.26. With air, the values will be $1/0.232 = 4.3$ times these values. Thus, the range of values for S is large. It turns out that the stoichiometric ratio affects the ratio of height of smolder zone to the stick diameter as will be brought out in section 8.

The measured values of T_s in the experiments by Moussa, Toong, and Garris (1977) and those made here (discussed below) show that with quiescent air, T_s is 1000 ± 50 K. Even in the case of packed bed of gasification of biomass or pellets, the measured surface temperature at low superficial velocities of around 0.03–0.04 m/s, T_s is around this value. With the use of oxygen, Yamazaki, Matsouka, and Nakamura (2018) have measured values of 1200 K for pure oxygen and intermediate values for lower fractions of oxygen in the smoldering regime. The data set out in references (Moussa 1976; Moussa, Toong, and Garris 1977; Yamazaki et al. 2019; Yamazaki, Matsouka, and Nakamura 2018; Yan et al. 2022) have been condensed into a functional fit as below. While the general feature is that, with air, most biomass show the measured surface temperature as 1030 ± 50 K and with oxygen fractions of $Y_{ox} = 0.6$, the measured values increase up to 1500 K, it was considered appropriate to relate it to oxygen fraction, ambient pressure that influences the availability of oxygen reacting with the char on the surface and the moisture and ash fractions of the incense stick as follows:

$$T_s = 680 + 930 Y_{ox} + 250(p_a/101)^{0.25} - 300(f_w + f_{ash}) \tag{17}$$

The choice of the constants has been made to reduce the deviation from known experimental data, and Figure 6 shows the calculated result from the above expression with the measured surface temperature. As can be noted, the scatter in the data at around 1000–1050 K is significant, even allowing for the accuracies in temperatures set at ±3%.

In order to further examine if the kinetic process is affecting the surface reaction, the dependence of the surface temperature on $\dot{r}$ and $\rho_f \dot{r}$ is set out in Figure 7.

It can be noted that the relationship of T_s with $\rho_f \dot{r}$ is superior to that with $\dot{r}$. The larger smoldering rates (130–170 g/m^{2}s) and surface temperature (1240–1340 K) are with higher fractions of oxygen, and surely in these cases diffusion rates can be considered controlling as the reaction rates are understood to be high. The spread of the data points around the smoldering rates in air around 1050 K implies that the factor other than kinetic process and in these cases, diffusion is indeed the controlling feature.

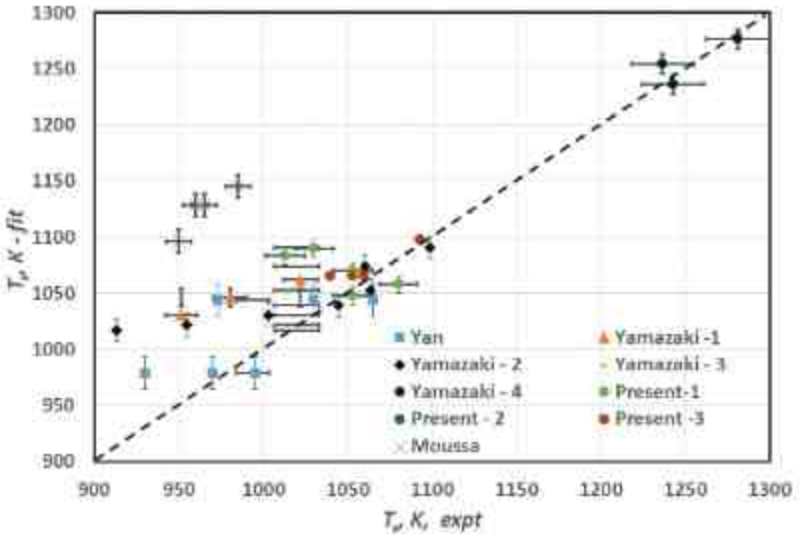

Figure 6. Comparison between the fit for surface temperature with the measured values from experiments.

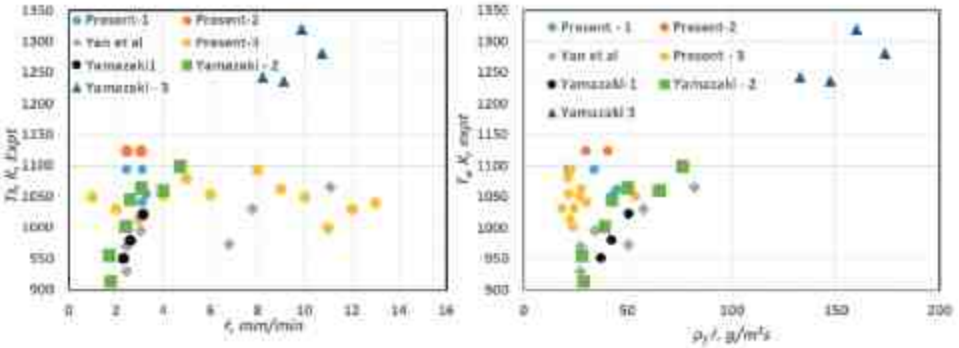

Figure 7. The plots of surface temperature with the linear smoldering rate, $\dot{r}$, and surface mass flux, $\rho_f \dot{r}$, from experiments.

Equations for smoldering rate

We can now set out the equations needed for calculating the smoldering rate.

$$\rho_f \dot{r} c_{pf}(T_s - T_0) = \frac{H_s}{d} D\rho Y_{ox} C_0 \left(1 + C_1 Gr^{1/4}\right) \tag{18}$$

We define similar to that in Mukunda et al. (2007),

$$Re_r = \rho_f \dot{r} d/\mu_g \tag{19}$$

We note that we can take $D_{12}\rho = \mu_g$, the equivalent of unity Schmidt number ($Sc = 1$). With the definition of B as in Equation 15, we get

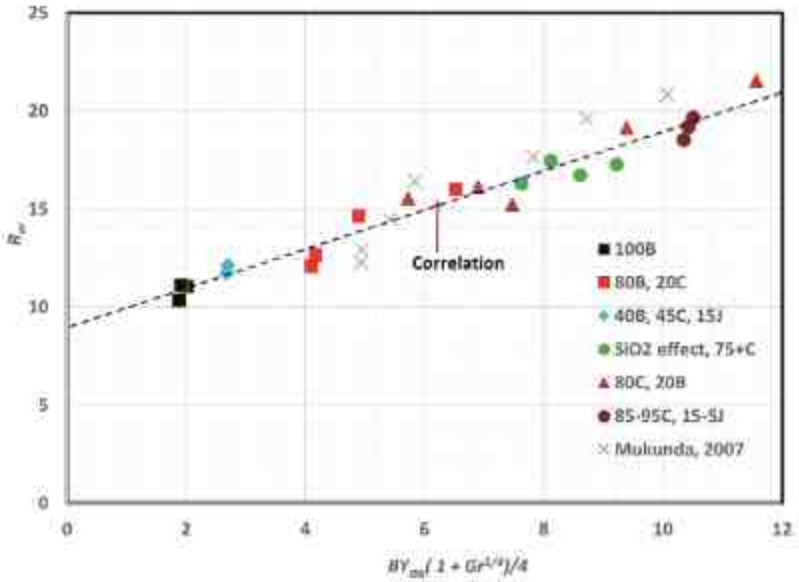

Figure 8. Comparison between the correlation and the experimental results on Re_r for the 20 compositions made at the laboratory.

$$Re_r = BY_{ox}C_0(1 + C_1 Gr^{1/4}) \tag{20}$$

The above relationship has constant C_0 and C_1. Data of compositions 1–27 in Table A1 were used to seek the best fit for the constants C_0 and C_1. Several ways of expressing the relationship that has wider fit of the data were explored. It was finally inferred that the fit would be best with $C_0 = C_1 = 1$ and, therefore,

$$Re_r = 9 + [BY_{ox}(1 + Gr^{1/4})/4] \tag{21}$$

Figure 8 presents a plot of the experimental data on Re_r for the specifically designed 20 compositions with the correlating parameter $BY_{ox}(1 + Gr^{1/4})/4$. Data of the present experiments follow the fit reasonably well. The comparison of experimental data and the predictions on Re_r is also shown in Tables A1 and A2, and it can be seen that the predictions are indeed very good for the specific compositions made at the laboratory and moderate for others.

Extension to low pressure behavior

Two studies that have examined low pressure and oxygen fraction behavior are by Moussa, Toong, and Garris (1977) and Yamazaki, Matsouka, and Nakamura (2018). The studies on cotton conducted by Moussa, Toong, and Garris (1977) are at a very low density (60 kg/m^3) and are in a horizontal configuration with the "stick or strand" laid on a fine metal mesh as described in Moussa (1976). The orientation and the metal mesh may have some contributions to the differences from the vertical unsupported condition. However, it is the smoldering process in an order-of-magnitude lower-density geometry with wider spaces between thinner fuel layers that may contribute to the three-dimensional stop–start ignition

phenomenon that on the average appears as a slower but steady regression. Nevertheless, their data are considered for comparisons with the model predictions here and also examined through specifically indicative experiments. The low-pressure model prediction strategy considered here uses, however, the data of Yamazaki, Matsouka, and Nakamura (2018) who experimented upon biomass sticks with an identified density of 970 kg/m^3, all of 2 mm diameter at various pressures below ambient and with different oxidizer fractions. Their data particularly for Y_{ox} at 0.20, 0.23 and 0.33 and various pressures below the ambient value have been used for analysis here, and some indicative data are set out in Table A5. Although the actual data set has 37 points at different Y_{ox} and p_a, the table shows the data for some select samples. The incense sticks obtained from commercial sources are stated to be made largely of sawdust. The values chosen for f_b, f_w and f_a are set out in Table A5 as also the measured surface temperatures. Their experiments indicated that beyond Y_{ox} of 0.33, the smoldering sticks would transition to combustion and this was far more significant at higher Y_{ox}.

Similar to the above, the data of Moussa (1976) drawn largely from a table of data set out in Appendix 2.1 of the thesis are set out in Table A6, which shows 10 of the points considered for analysis here.

Data at various Y_{ox} and p_a are examined to seek a correlation for the oxidizer fraction and pressure effects. Both Yamazaki, Matsouka, and Nakamura (2018) and Moussa (1976) indicate that the oxidizer mass fraction effect is much stronger than pressure – an aspect that is brought out from the analysis here. An important point to notice is that since geometry involves a duct and a suction process to maintain the pressure, it can be inferred that there could be some forced convection. The only way of inferring this feature for the present study is to assume a small value of flow velocity alongside the stick and account for the effect of forced convection in the present correlation. In the present case, a velocity of 0.05 m/s is assumed. The analysis starting with a plot of the experimental Re_r with $ln(101/p_a)$ is set out on the left side of Figure 9.

It is noted that the variations are linear, and the data on the left side of Figure 9 can be set out into the following curve fits. While these are excellent representations for the data for $Y_{ox} = 0.2$, 0.23 and 0.33, they become less and less representative for $Y_{ox} = 0.53$ and 1.0.

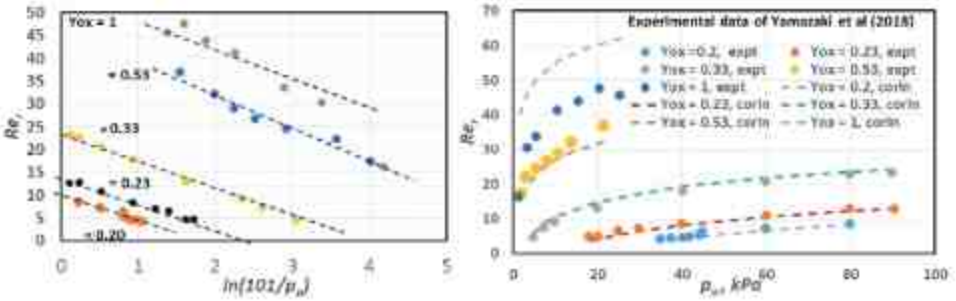

Figure 9. The left part has the variation of Re_r with $\ln(101/p_a)$ and the right part has the comparison of the correlation with the experimental data of Yamazaki, Matsouka, and Nakamura (2018).

$$Re_r = 10 - 6ln(101/p_a) \quad \text{for } Y_{ox} = 0.20 \tag{22}$$

$$Re_r = 14 - 6ln(101/p_a) \quad \text{for } Y_{ox} = 0.23 \tag{23}$$

$$Re_r = 34 - 6ln(101/p_a) \quad \text{for } Y_{ox} = 0.33 \tag{24}$$

$$Re_r = 40 - 6ln(101/p_a) \quad \text{for } Y_{ox} = 0.53 \tag{25}$$

$$Re_r = 55 - 6ln(101/p_a) \quad \text{for } Y_{ox} = 1.00 \tag{26}$$

The constants varying with Y_{ox} can be fitted into $Re_r = 55 + 28ln(Y_{ox})$ to get

$$Re_r = 55 + 28ln(Y_{ox}) + 6ln(p_a/101) \tag{27}$$

By replacing the constant 55 by $9 + [BY_{ox}(1 + Gr^{1/4})/4]$ and minor algebra, the data can be condensed into an expression

$$Re_r = [9 + (BY_{ox}(1 + Gr^{1/4})/4)]\ ln[e(Y_{ox}/0.23)^2(p_a/101)^{0.43}] \tag{28}$$

rearranged in such a manner that at $Y_{ox} = 0.23$ and $p_a = 101\ kPa$, the earlier fit as in Equation 21 is obtained. If flow Reynolds number correction is added (with its constant as 0.1), as may be required in the case of experiments of Yamazaki, Matsouka, and Nakamura (2018) (to be discussed below), we can finally write the correlation as

$$Re_r = [9 + (BY_{ox}(1 + Gr^{1/4})/4)]\ ln[e(Y_{ox}/0.23)^2(p_a/101)^{0.43}][1 + 0.1Re^{0.5}] \tag{29}$$

A comparison between the results of correlation on Re_r and the experimental data set out on the right side of Figure 9 shows that for $Y_{ox} = 0.2$, 0.23 and 0.33, the correlation appears good. Deviations for $Y_{ox} = 1$ are significant and may need a special consideration not thought important here as at this condition since the smouldering stick transitions to flaming largely.

After having ensured the availability of a correlation to compare well with the experimental results, the results of Moussa (1976) and Yamazaki, Matsouka, and Nakamura (2018) are set out in Figure 10. It can be seen that the results of Moussa (1976) are over-predicted with a scaling factor of 1.4. This led to further exploration. In order to pursue the speculation of an irregular smoldering process, experiments were made with strands and lit at the top. One of these experiments performed on a 25 *mm* diameter strand at a density of 70 kg/m^3 is presented in Figure 11. The first picture of smoldering bleached cotton strand shows that it has halted just after ignition. Being different from this, the natural cotton strands are smoldering, but the char layer is progressing in various directions around the azimuth and in the central regions and the behavior that is seen is strongly dependent on the local density – some segments with lower than the mean and some slightly higher as physically observed. This random arrangement causes a local brush moving in some directions consuming that specific segment, followed by a wait and a sudden burst of a smoldering hot zone elsewhere. This phenomenon is considered responsible for lower average smoldering rate. Since most higher-density incense stick smoldering occurs smoothly in rgw vertical direction, no further attempt is made to deal with the data of Moussa (1976).

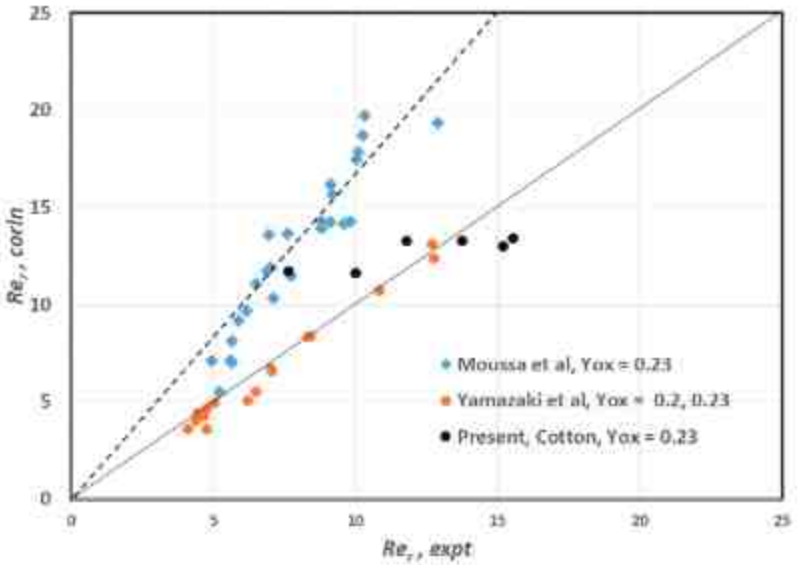

Figure 10. Comparison of Re_f between correlation and experiments for Yamazaki, Matsouka, and Nakamura (2018) and Moussa (1976).

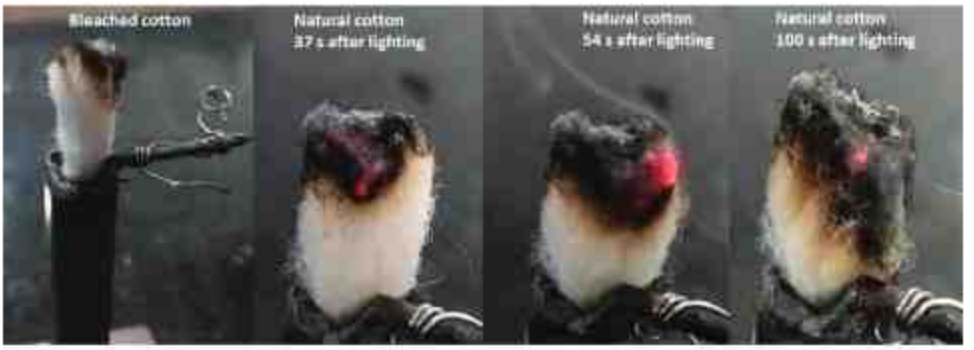

Figure 11. Pictures of smouldering of cotton strand, d =25 mm, $\rho_f = 70\ kg/m^3$ at different times.

Comparison of results with those of Lin, Chow, and Huang (2021)

Lin, Chow, and Huang (2021) conducted experiments on incense sticks made from powders of sage and cedar at three diameters of 1.5, 2.5 and 5.0 mm with $\rho_f = 720\ kg/m^3$ and samples with $\rho_f = 720$, 920 and 1,100 kg/m^3 at $d = 1.5\ mm$ at different stream speeds. Here, we consider the results at zero speed with what they have termed "opposed configuration", which is the same as in Figure 1. The experimental results of the six cases and the predictions are set out in Table A7. As can be noted except for the first case, other predictions are reasonable. The issue with the data is that the density values are set out as nominal values. It is the experience of the present authors that in working with natural materials and processing them, there will be inevitable variations in size and hence the density that depends on the square of the size can vary between samples. As it appears, the comparisons are good but could be expected to be better with the availability of the actual composition and density data.

Comparison with results on char cylinders of Yan et al. (2022)

Yan et al. (2022) conducted studies on char rods from (a) a mixture of cypress powder mixed with elm bark powder and (b) elm bark powder produced in their laboratory at different diameters (2, 4 and 6 *mm*); they have provided the compositional details also. They have measured the smolder rate, surface temperature and also the shape of the geometry after quenching the steadily smoldering stick. The shapes are assessed as height-to-diameter ratio. These data are set out in Table A8. With regard to the smoldering rates, except in two cases, there is substantial difference between the results of experiments and the correlation. This is perhaps related to the composition and density. In the experience of the present authors, extruding materials of different diameters to identical densities is a very difficult task and significant differences may be found in the density achieved in each of the samples. Since the density has a direct impact on Re_r, the comparison may improve with data on individual cylinders.

Cone shape of the steady smoldering front

Yan et al. (2022) have taken efforts to describe the shape of the cone of the steady propagating front of char cylinders. The shapes of the steady front have been photographed by Lin, Chow, and Huang (2021). They invoke similarity of the behavior between the volumetric flow rate of methane–air flame with height and the mass flow rate of the char with height of the cone. The relationship set out by them does not provide an independent way of determining the flame height. A more effective simple overall analysis provided in Mukunda (2009) indicates that the height of the flame is proportional to the stoichiometric ratio. It would be interesting to explore this. To obtain more data on the role of stoichiometric ratio, the smoldering of several incense sticks was quenched and the cone height was measured. Figure 12 shows the photographs of the sticks quenched after they reached a steady smoldering condition.

Case 1 – 100 B
d = 2.9 mm
h/d = 1.38

Case – 2, 100 B
d = 3.2 mm
h/d = 1.7

Case – 15, 80 C+ 20 B
d = 3.0 mm
h/d = 3.87

Case – 20, 95 C+ 5 B
d = 6.2 mm
h/d = 4.05

Figure 12. Photographs of the quenched smouldering sticks from biomass to char.

It is clear from the photographs that the cones are much shallower for biomass than for char. The values of h/d of these are set out in Table A1. The values of h/d of Lin, Chow, and Huang (2021) were obtained by making measurements of the photographs and set out in Table A7, and those reported by Yan et al. (2022) are set out in Table A8. Figure 13 shows the plot of h/d with stoichiometric ratio. The variation of most of the data can be considered to follow a linear behavior that can be described by $h/d = S/2$. The fact that some of the data of Yan et al. (2022) fall below the line might be indicative of the experimental procedure used to extract the data. An additional support in favor of the dependence on stoichiometry was obtained from an experiment (not reported here) that was conducted to explore the flow effects by placing downward smoldering sticks in a tube with air flow coming downwards. When the steady burn was obtained at higher speed, the value of h/d remained unaltered, indicating that the ash layer had no influence on the formation of the cone. The rate of consumption of the char allowed the formation of the cone depending on the stoichiometry. An examination of the data presented in Table A1 shows that there is no further dependence of h/d on d as suggested by Yan et al. (2022).

Extinction of smoldering sticks

There are two ways in which extinction of smoldering sticks are caused: (a) composition and (b) reduction in a combination of ambient pressure and oxygen fraction. The first one has been uncovered as a possibility because of the inadvertent introduction of a compound that decomposes endothermically at temperatures close to the surface temperature of a smoldering stick. It has been determined (Sowriraajan et al. 2023) that the presence of termite mud/clay contains compound "antigorite" as also quartz sand, causing two

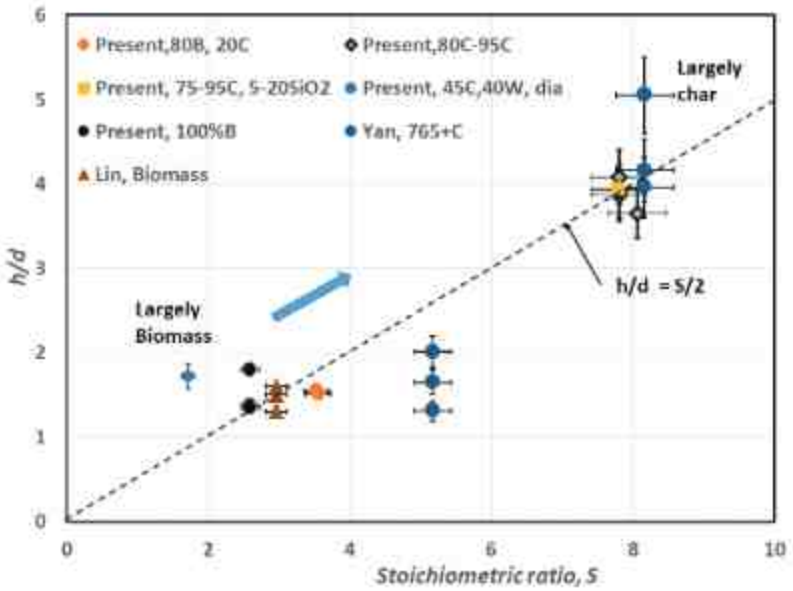

Figure 13. The variation of the cone height-to-diameter ratio with the calculated stoichiometric ratio.

Table 2. Details of extinguishment of smouldering sticks: $\dot{r}$ at extinction is 1.5 ± 0.1 mm/min and Re_r is 2–4.

No	ρ_f	f_{eff}	Y_{ox}	p_a kPa	T_s Exp, K	Cause	Ref.
27	800	0.305	0.23	101	800	Composition	Sowriraajan et al. (2023)
69	970	0.252	0.20	− 35		Lowering p_a, Y_{ox}	Yamazaki, Matsouka, and Nakamura (2018)
77	970	0.252	0.23	− 18	913	Lowering p_a	Yamazaki, Matsouka, and Nakamura (2018)
126	60	0.288	0.16	− 132	880	Lowering Y_{ox}	Moussa (1976)

effects – endothermic decomposition of antigorite and the naturally occurring α-quartz that undergoes endothermic phase transformation to β-quartz at temperatures of 800 K or above that. Both these draw away the heat from the exothermic surface reaction. If the incense stick has a low nominal burning rate caused by the presence of inorganic compounds (ash) and has an inadvertent introduction of additional compounds such as described here, it will inevitably extinguish. The entire process is transient starting with larger energy with a flame-lit stick. Over a certain period of time that may last a few hundred seconds; there will be a reduction in surface temperature (brought out in Sowriraajan et al. 2023) until a point when the smolder will extinguish.

Table 2 contains the four cases of extinction around the data discussed earlier. In the case of reduction in Y_{ox} or p_a (as in the three cases in the table), the system evolves so as to balance the exothermic surface reaction with the heat transfer to the condensed phase at lower smoulder speed. However, below a certain condition, the condensed phase continues to demand heat transfer at a rate wherein the surface temperature cannot sustain the heat release, simply because of the reduction in the magnitude of the surface reaction. The transient reduction in surface temperature follows the behavior as described in the earlier case (Sowriraajan et al. 2023) and hence extinction results. One can notice that the surface temperature is about 800–900 K at a condition where any trigger toward reduced heat release leads to extinction. An approach to determine the fundamental controlling factor was conceived as the smoulder Reynolds number, Re_r. Figure 14 shows the plot of measured T_s with Re_r. It can be seen that the temperature drops toward lower Re_r, and the result of Sowriraajan et al. (2023) that corresponds to case 27 and the indications of other conditions leading to extinction seem to be consistent with the expectation that the surface temperature is between 800 K and 900 K and Re_r is between 2 and 4. Extinction is always a zone since many micro-features contribute to it and these vary even from sample to sample.

Discussion and final remarks

The relationships needed to obtain the smoldering rate are set out as below. To understand the role of various independent parameters, Equation 29 is set out in terms of $\dot{r}$ for the case, $p_a = 101\ kPa$.

$$f_{eff} = f_c + 0.3 f_b \tag{30}$$

$$T_s = 1144 + 930(Y_{ox} - 0.23) - 300(f_w + f_{ash}) \tag{31}$$

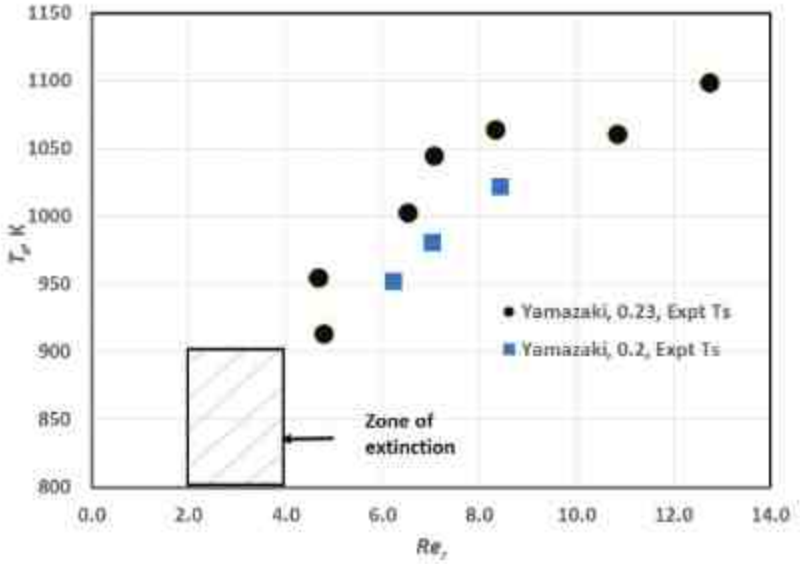

Figure 14. The plot of surface temperature vs. Re_f showing the possible extinction region.

$$H_s = f_{eff}\frac{9.2C_{00}+32.8}{1+C_{00}} \tag{32}$$

$$C_{00} = 0.75\exp[-5000(1/1000-1/T_s)] \tag{33}$$

$$\dot{r} = \frac{\mu}{\rho_f}\left[\frac{9}{d}+\frac{H_s Y_{ox}^2}{c_{pf}(T_s-T_0)4d}\left(1+\left(\frac{g(1-T_0/T_s)d^3}{(\mu/\rho)^2}\right)^{1/4}\right)\right]\left[1+2ln\left[\frac{Y_{ox}}{0.23}\right]\right] \tag{34}$$

Figure 15 is a composite of several parameters, namely, f_{eff}, T_s, H_s and B that are set out for compositions 1–20. The effective fuel constituting the char is the lowest for the biomass and increases toward the char. Dips will be related to additional ash in the composition (as it happens in the case of Yan et al. 2022). The surface temperature, T_s, varies around 1000–1100 K weakly dependent on whether the composition is wholly biomass or char because it is the char that is smoldering with ash fraction up to 17%. This is reflective of the diffusional dominance of the smoldering process. The heat of surface reaction is dependent on the magnitude of the effective fuel and the fraction of CO to CO_2. The relative fraction is a function of temperature. The CO/CO_2 ratio varies between 0.50 and 0.53 in this region. While this also contributes to the evaluation of H_s, the stronger dependence of H_s comes from f_{eff}. This is the reason that the variation of H_s follows the pattern of f_{eff}. The variation of B is the same as of H_s. The expression for smoldering rate has the inverse dependence on fuel density, an aspect that need not be overstated, but earlier literature does not account for it adequately. Indeed, if it were so, the data presentation on incense sticks would have included the mass flux, $\rho_f \dot{r}$, instead of $\dot{r}$

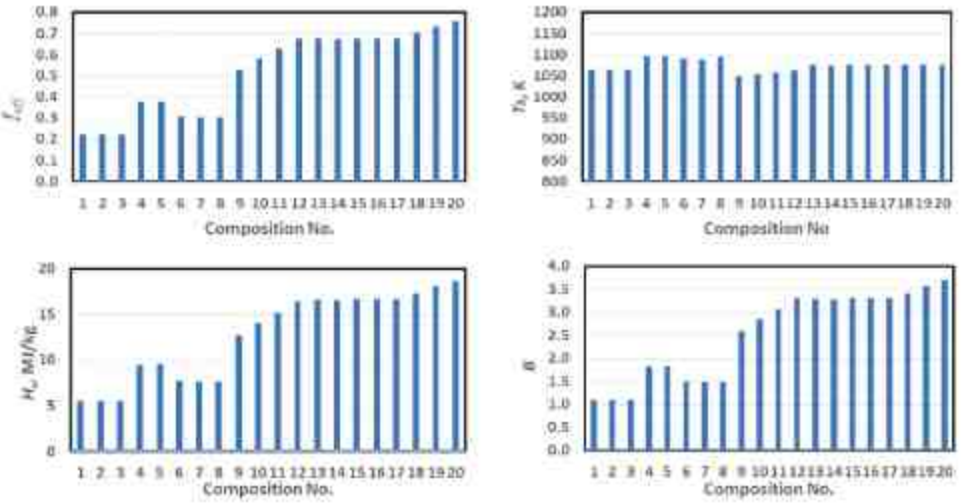

Figure 15. The plots of f_{eff}, T_s, H_s and B for compositions 1–20.

alone, or perhaps the adoption of smolder Reynolds number, Re_r, which would be most appropriate as in Mukunda et al. (2007) (Yamazaki, Matsouka, and Nakamura (2018) just defines it).

The dependence of $\dot{r}$ on d is interesting. A segment that has a strong dependence $1/d$ and another $1/d^{1/4}$ coming from the Grashof number dependence. A test of this dependence comes from comparison with the results of Lin, Chow, and Huang (2021) with compositions 28, 29 and 30. The weak comparison on composition 28 is argued to be due to the actual density of this sample departing from the nominal.

A comparison of the data from multiple sources along with the present correlation of 85 different data sets is presented in Figure 16. Even though the low-density data of cotton by Moussa (1976) are excluded from the plot on the basis of discussion set out earlier, specific higher density data on cotton from experiments conducted at the laboratory are included. Also, the data of Yamazaki, Matsouka, and Nakamura (2018) at $Y_{ox} = 0.53$ and 1.0 are excluded, since these are considered closer to the combustion mode. The correlation based on simple scaling principles and ensuring the consistency with the experimental observations seems to compare very well with the data from a number of sources. A part of the differences is the lack of the needed basic information on composition and density of the incense sticks which, if resolved, would lead to improved comparison. Finally, the correlation that includes extinction features is set out as

$$Re_r = [9 + (BY_{ox}(1 + Gr^{1/4})/4)]\ ln[e(Y_{ox}/0.23)^2(p_u/101)^{0.43}][1 + Re_u^{0.5}]H(X) \qquad (35)$$

where $X = (Re_r - Re_{rc})$ is the Heaviside step function that is 1 for $Re_r > Re_{rc}$ and 0 for $Re_r < Re_{rc}$. The value of Re_{rc} is taken as 3, with an understanding that the extinction region is $Re_r = 3 \pm 1$. A minor aspect of the predictions is that the shape of the smoldering surface is related to the stoichiometric ratio - $h/d = S/2$.

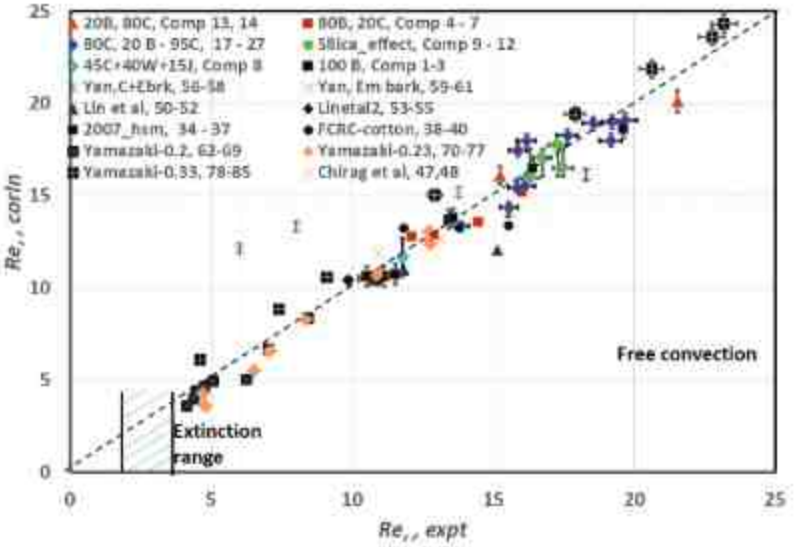

Figure 16. The comparison between the results of correlation with experiments ($Re_r, corrln = [9 + BY_{ox}(1 + Gr^{1/4})/4)]\ ln[e(Y_{ox}/0.23)^2(p_u/101)^{0.43}][1 + Re_u^{0.5}]$).

List of symbols

B	Transfer number $= H_s/[c_{pf}(T_s - T_0)]$
C_{pf}, C_{pg}	Specific heats of solid fuel and gas phase (kJ/kgK)
d	Char cone diameter (m)
Σ_{ox}	Diffusion coefficient of oxidizer (m^2/s)
f_b	Biomass fraction (with jigit and/or guar gum treated as biomass)
f_c	Char fraction
f_w	Moisture fraction
f_{ash}	Ash fraction
f_{eff}	Effective fuel defined in Equation 1
Gr	Grashof number defined in Equation 8
h	Char cone height (m)
H_0	Heat of combustion (MJ/kg)
H_s	Surface heat release (kJ/kg)
k_f	Thermal conductivity of the fuel (W/mK)
$\dot{m}_{f,ox}$	Fuel or oxidizer mass flow rate (kg/s)
r	Smoldering rate (mm/min)
Re_u	Flow Reynolds number defined on Equation 8
Re_r	Smoldering Reynolds number
Re_{rc}	Smoldering Reynolds number at extinction
S	Stoichiometric ratio
T_s	Surface temperature (K)
T_0	Core initial temperature (K)
Y_{ox}	Oxidizer fuel fraction in the ambient (K)
ρ_f	Density of fuel (kg/m^3)
α_f	Thermal diffusivity of fuel (m^2/s)
ρ	Density of oxidizer (kg/m^3)
$H(X)$	Heaviside step function
μ_g	Ambient gas phase viscosity (kg/ms)

Acknowledgements

The authors are thankful to the authorities of Jain (deemed-to-be-university) for encouragement to perform this study.

Disclosure statement

No potential conflict of interest was reported by the author(s).

References

Baker, R. R. 1977. Combustion and thermal decomposition regions in a burning cigarette. *Combust. Flame* 30:21–32. doi:10.1016/0010-2180(77)90048-7.

Chirag, K. M., K. Vijay, V. Raghavan, and A. S. Rangwala. 2011. Smoldering combustion of biomass particles. *J. Appl Sci.* 11 (10):1862–66. doi:10.3923/jas.2011.1862.1866.

Dupont, C., R. Chiriac, G. Gauthier, and F. Toche. 2014. Heat capacity measurements of various biomass types and pyrolysis residues. *Fuel* 115:644–51. doi:10.1016/j.fuel.2013.07.086.

Lin, S., T. H. Chow, and X. Huang. 2021. Smoldering propagation and blow-off on consolidated fuel under external airflow. *Combust. Flame* 234:234. doi:https://doi.org/10.1016/j.combustflame.2021.111685.

Liu, Y., and R. He. 2015. Variation of apparent reaction order in char combustion and its effect on a fractal char combustion model. *Combust Sci. Technol.* 187 (10):1638–60. doi: 10.1080/00102202.2015.1059327; see also He, W., He, R., Ito, T., Suda, T., and SatoJ. 2011. Numerical investigations of CO/CO_2 ratio in char combustion. Combust. Sci. Technol. 183:868-882.

Momeni, M., C. Yin, S. K. Kær, T. B. Hansen, P. A. Jensen, and P. Glarborg. 2012. Experimental study on effects of particle shape and operating conditions on combustion characteristics of single biomass particles. *Energ. Fuel.* 27 (1):507–14. doi:10.1021/ef301343q.

Moussa, N. A. 1976. Mechanism of smouldering combustion in cellulosic materials. Ph.D Diss, Massachusetts Institute of Technology.

Moussa, N. A., T. Y. Toong, and C. A. Garris. 1977. *Mechanism of smouldering of cellulosic materials. Sixteenth symposium (international) on combustion*. Pittsburgh: The Combustion Institute.

Mukunda, H. S. 2009. *Understanding combustion*. 2nd ed. India: Universities press.

Mukunda, H. S. 2011. *Understanding clean energy and chemicals from biomass*. India: Wiley.

Mukunda, H. S., J. Basani, H. M. Shravan, and B. Philip. 2007. Smoldering combustion of "incense" sticks – experiments and modeling. *Combust Sci. Technol.* 179 (3):1113–29. doi:10.1080/00102200600970019.

Peterson, C. A., and R. C. Brown. 2020. Oxidation kinetics of biochar from woody and herbaceous biomass. *Chem. Engg. J.* 401:401. doi:10.1016/j.cej.2020.126043.

Ragland, K. W., D. J. Aerts, and A. J. Baker. 1991. Properties of wood for combustion analysis. *Bioresour. Technol.* 37 (2):161–68. doi:10.1016/0960-8524(91)90205-X.

Ranz, W. E., and W. R. Marshall. 1952. Evaporation from drops. *Chem. Eng. Prog.* 48:141–46.

Rein, G. 2009. Smoldering combustion phenomena in science and technology. *Int. Rev. Chem. Eng.* 1:3–18.

Sowriraajan, A. V., A. Shivakumar, P. Sachin, C. S. Bhaskar Dixit, and H. S. Mukunda. 2023. Investigations of self-extinction of incense sticks. *Fire Technol.* 59 (4):1449–64. doi:10.1007/s10694-023-01389-5.

Torero, J. L., J. I. Gerhard, M. J. Martins, M. A. B. Zanoni, T. L. Rashwan, and J. K. Brown. 2020. Processes defining smouldering combustion: Integrated review and synthesis, Prog. *Energ. Combust. Sci.* 81:100869. doi:10.1016/j.pecs.2020.100869.

Varunkumar, S., N. K. S. Rajan, and H. S. Mukunda. 2011. Single particle and packed bed combustion in modern gasifier stoves—density effects. *Combust Sci. Technol.* 183 (11):1147–63. doi:10.1080/00102202.2011.576658.

Varunkumar, S., N. K. S. Rajan, and H. S. Mukunda. 2013. Universal flame propagation behavior in packed bed of biomass. *Combust Sci. Technol.* 185 (8):1241–60. doi:10.1080/00102202.2013.782297.

Yamazaki, T., T. Matsouka, and Y. Nakamura. 2018. Near-extinction behaviour of smouldering combustion under highly vacuumed environment. *Proc. Combust. Inst.* 1–8. doi:https://doi.org/10.1016/j.proci.2018.06.200.

Yamazaki, T., T. Matsouka, Y. Nakamura, and Y. Li. 2019. Applicability of a low-pressure environment to investigatesmoldering behavior under microgravity. *Fire Technol.* 56 (1):209–28. doi:https://doi.org/10.1007/s10694-019-00911-y.

Yan, S., F. Jem, J. Cai, P. Sun, Y. Zhang, F. Benrendt, and A. Dieguez-Alonso. 2022. Characteristics of char cone covered by ash in steady smouldering of a char rod. *Combust Sci. Technol.* 1–10. doi:https://doi.org/10.1080/00102202.2022.2150079.

Appendices

Table A1. Composition and basic data of incense sticks and measured smoldering data, $Y_{ox} = 0.232$, ambient pressure, $p_a = 95$ kPa, B = biomass, C = char, ga-M = guar gum.

No.	Type	f_b	f_c	f_w	f_{ash}	f_{eff}	ρ_f kg/m³	d mm	$\dot{r}$ mm/min	$\rho_f \dot{r}$ g/m²s	t/d
1	100 B,1	0.751	0	0.092	0.157	0.225	778	2.9	3.31	43.5	1.38
2	100 B,2	0.751	0	0.092	0.157	0.225	820	3.2	3.15	43.1	1.80
3	100 B,2	0.751	0	0.092	0.157	0.225	853	3.0	3.16	44.9	1.35
4	80B, 20C	0.751	0.083	0.083	0.082	0.309	443	5.9	3.33	24.6	1.52
5	80B, 20C	0.747	0.083	0.083	0.081	0.307	480	7.7	2.85	22.8	1.55
6	80B, 20C	0.686	0.172	0.051	0.091	0.377	530	8.7	2.50	22.1	
7	80B, 20C	0.689	0.172	0.047	0.092	0.379	655	4.5	3.15	34.4	
8	55B, 45C	0.710	0.123	0.103	0.064	0.336	885	3.2	3.00	44.3	1.72
9	20SiO2-C	0.035	0.520	0.036	0.271	0.530	864	6.2	2.20	31.7	3.24
10	15SiO2-C	0.036	0.571	0.041	0.245	0.581	952	6.0	2.20	34.9	3.49
11	10SiO2-C	0.036	0.617	0.044	0.231	0.628	815	5.9	2.49	33.8	3.62
12	05SiO2-C	0.037	0.667	0.045	0.214	0.678	760	6.0	2.75	34.8	3.94
13	80C, 20B	0.158	0.628	0.040	0.174	0.676	730	8.5	2.50	30.4	
14	80C, 20B	0.156	0.626	0.044	0.174	0.673	786	4.5	3.10	40.6	
15	80C, 20B	0.158	0.631	0.041	0.170	0.678	711	3.0	5.30	62.8	3.87
16	80C, 20B	0.158	0.631	0.041	0.170	0.678	735	4.0	4.00	49.0	3.92
17	80C, 20B	0.158	0.631	0.041	0.170	0.678	712	6.3	3.10	36.8	4.08
18	85C, 15B	0.118	0.666	0.046	0.170	0.701	681	6.9	2.86	32.5	3.65
19	90C, 10B	0.079	0.708	0.041	0.171	0.732	725	6.6	2.97	35.9	3.80
20	95C, 5B	0.039	0.747	0.042	0.171	0.759	735	6.2	3.05	37.4	4.05
21	CG	0.446	0.365	0.067	0.122	0.499	900	3.1	3.60	54.0	
22	G-1-Ga-M	0.410	0.410	0.027	0.154	0.533	668	8.6	2.20	24.5	
23	G-2 -Ga-M	0.399	0.399	0.066	0.136	0.519	850	8.6	1.60	22.7	
24	G-3-Ga-M	0.376	0.377	0.114	0.133	0.489	900	8.5	1.50	22.5	
25	C-1-Sand	0.324	0.267	0.038	0.250	0.365	684	8.7	1.91	21.8	
26	C-2-Sand	0.258	0.211	0.038	0.282	0.288	717	8.8	1.83	21.9	
27	C-3-Te-M	0.272	0.223	0.037	0.266	0.305	800	8.5	Ext	Ext	

Table A2. Composition and basic data of incense sticks and measured smoldering data, $Y_{ox} = 0.232$, ambient pressure, $p_a = 96$ kPa, B = biomass, C = char, cot = cotton, a-1, b-1, c-1 and d-1 = data from Mukunda et al. (2007).

No.	Type	f_b	f_c	f_w	f_{ash}	f_{eff}	ρ_f kg/m³	d mm	$\dot{r}$ mm/min	$\rho_f \dot{r}$ g/m²s
28	C-4	0.849	0.000	0.044	0.106	0.255	600	8.8	2.3	23.0
29	C-5	0.116	0.657	0.050	0.178	0.692	770	8.8	2.2	28.2
30	C-6	0.438	0.359	0.044	0.159	0.490	662	8.8	2.5	27.6
31	C-7	0.479	0.319	0.050	0.152	0.463	657	8.7	2.2	24.1
32	C-8	0.665	0.166	0.053	0.116	0.366	591	8.7	1.9	18.8
33	C-9	0.268	0.500	0.055	0.177	0.580	706	8.7	2.6	30.6
34	a-1	0.446	0.365	0.067	0.122	0.499	1150	3.5	2.4	46.0
35	b-1	0.446	0.365	0.067	0.122	0.499	1100	3.6	2.6	47.4
36	c-1	0.446	0.365	0.067	0.122	0.499	900	7.0	1.9	28.1
37	d-1	0.446	0.365	0.067	0.122	0.499	800	10.0	1.8	23.5
38	Cot-1	0.960	0.000	0.04	0.02	0.288	87	6.8	14.3	20.8
39	Cot-2	0.960	0.000	0.04	0.02	0.288	147	6.9	9.7	23.8
40	Cot-3	0.960	0.000	0.04	0.02	0.288	220	7.2	7.0	25.8
41	Cot-4	0.960	0.000	0.04	0.02	0.288	260	3.5	6.1	26.3
42	Cot-5	0.960	0.000	0.04	0.02	0.288	329	3.3	6.7	36.5
43	Cot-6	0.960	0.000	0.04	0.02	0.288	401	6.6	4.2	27.8

Table A3. The calculated parameters for the model on smoldering rate and comparison, expt = experiment, corln = correlation, rat = ratio of CO to CO_2.

No.	Type	f_{eff}	S	T_s K	Rat	H_s MJ/kg	B	$Gr^{1/4}$	Re_f Expt	Re_f Corln	Error %
1	100 B, 1	0.225	2.6	1069	0.54	5.5	1.1	5.84	10.5	10.6	<5
2	100 B, 2	0.225	2.6	1069	0.54	5.5	1.1	6.30	11.5	10.7	−5
3	100 B, 3	0.225	2.6	1069	0.54	5.5	1.1	5.95	11.1	10.6	<5
4	80B,20C	0.309	3.5	1094	0.49	7.7	1.5	10.0	12.1	12.8	+6
5	80B,20C	0.307	3.5	1093	0.49	7.7	1.5	12.2	14.7	13.9	−6
6	80B,20C	0.377	4.3	1101	0.47	9.5	1.8	13.3	16.0	15.5	<5
7	80B,20C	0.379	4.4	1098	0.48	9.5	1.8	8.2	12.9	12.9	<5
8	55B,45C	0.336	3.5	1098	0.48	7.7	1.5	6.3	11.8	11.7	<5
9	20SiO2-C	0.530	6.1	1062	0.56	12.9	2.6	10.3	16.3	16.6	<5
10	15SiO2-C	0.581	6.7	1065	0.55	14.2	2.8	10.1	17.5	17.1	<5
11	10SiO2-C	0.628	7.2	1058	0.55	15.3	3.1	10.0	16.7	17.0	<5
12	05SiO2-C	0.678	7.8	1069	0.54	16.6	3.3	10.0	17.3	17.7	<5
13	80C,20B	0.676	7.8	1080	0.52	16.7	3.3	13.1	21.5	20.6	<5
14	80C,20B	0.673	7.7	1079	0.52	16.6	3.3	8.1	15.2	16.1	+6
15	80C,20B	0.678	7.8	1080	0.52	16.8	3.3	6.0	15.5	14.7	−6
16	80C,20B	0.678	7.8	1080	0.52	16.8	3.3	7.4	16.1	15.9	<5
17	80C,20B	0.678	7.8	1080	0.52	16.8	3.3	10.4	19.2	18.4	<5
18	80C,20B	0.701	8.1	1079	0.52	17.3	3.4	11.1	18.5	18.9	<5
19	80C,20B	0.732	8.4	1080	0.52	18.1	3.6	10.8	19.7	19.5	<5
20	80C,20B	0.759	8.7	1080	0.52	18.8	3.7	10.3	19.2	19.0	<5
21	CG	0.499	5.7	1087	0.50	12.4	2.4	6.11	13.9	13.3	<5
22	G-1-Ga-M	0.533	6.1	1090	0.50	13.3	2.6	13.2	17.6	18.2	<5
23	G-2-Ga-M	0.519	6.0	1083	0.51	12.9	2.5	13.1	16.2	17.9	+11
24	G-3-Ga-M	0.489	5.6	1070	0.54	12.0	2.4	13.0	15.9	17.4	+10
25	C-1-Sand	0.365	4.2	1058	0.57	8.8	1.8	13.3	15.8	15.4	<5
26	C-2-Sand	0.288	3.3	1048	0.60	6.9	1.4	13.4	16.0	14.1	−12
27	C-3-Te-M	0.305	3.3	Ext	Ext	0	0	13.4	Ext	Ext	

Table A4. The calculated parameters for the model on smoldering rate and comparison, expt = experiment, corln = correlation, rat = ratio of CO to CO_2, a-1, b-1, c-1 and d-1 = Mukunda et al. (2007).

No.	Type	f_{eff}	S	T_s K	Rat	H_s MJ/kg	B	$Gr^{1/4}$	Re_f Expt	Re_f Corln	Error %
28	C-4	0.255	2.9	1099	0.48	6.4	1.2	13.4	16.8	13.4	−20
29	C-5	0.692	8.0	1076	0.53	17.0	3.4	13.5	20.8	21.3	<5
30	C-6	0.490	5.6	1083	0.51	12.2	2.4	13.4	20.2	17.6	−13
31	C-7	0.463	5.3	1083	0.51	11.5	2.3	13.3	17.5	17.1	<5
32	C-8	0.366	4.2	1074	0.49	9.2	1.8	13.4	13.7	15.3	12
33	C-9	0.580	6.7	1040	0.53	14.3	2.8	13.3	22.2	19.2	−14
34	a-1	0.499	5.7	1087	0.50	12.4	2.4	6.8	13.4	13.7	<5
35	b-1	0.499	5.7	1087	0.50	12.4	2.4	6.9	13.6	13.8	<5
36	c-1	0.499	5.7	1087	0.50	12.4	2.4	11.4	16.4	16.5	<5
37	d-1	0.499	5.7	1087	0.50	12.4	2.4	14.9	19.6	18.6	−5
38	Cot-1	0.960	3.3	1126	0.43	7.4	1.4	11.2	11.8	13.2	+12
39	Cot-2	0.960	3.3	1126	0.43	7.4	1.4	11.4	13.8	13.3	<5
40	Cot-3	0.960	3.3	1126	0.43	7.4	1.4	11.7	15.6	13.4	−14
41	Cot-4	0.960	3.3	1126	0.43	7.4	1.4	6.8	7.7	11.7	+53
42	Cot-5	0.960	3.3	1126	0.43	7.4	1.4	6.5	10.0	11.6	+15
43	Cot-6	0.960	3.3	1126	0.43	7.4	1.4	10.9	15.2	13.0	−15

Table A5. Composition and performance of incense sticks of Yamazaki, Matsouka, and Nakamura (2018) at different ambient pressures and oxygen fractions, $d = 2\ mm$, $\rho_f = 970\ kg/m^3$, $f_b = 0.84$, $f_w = 0.05$ and $f_{ash} = 0.11$, stream speed = 0.05 m/s, $Re_a = 8.3$.

No.	f_{eff}	Y_{ox}	p_a kPa	S	B	$\dot{r}$ mm/min	T_s Exp, K	Re_r Exp	Re_r Corlin	Error %
62	0.252	0.20	80.0	3.32	1.1	3.13	1022	8.4	8.36	<5
63	0.252	0.20	60.0	3.32	1.1	2.61	980	7.0	6.69	<5
64	0.252	0.20	45.0	3.32	1.1	2.31	952	6.2	5.03	−20
69	0.252	0.20	35.0	3.33	1.1	1.53		4.1	3.58	−13
70	0.252	0.23	90.5	2.90	1.2	4.72		12.7	13.1	<5
71	0.252	0.23	80.0	2.90	1.2	4.73	1099	12.8	12.4	<5
72	0.252	0.23	60.0	2.90	1.2	4.03	1060	10.9	10.7	<5
73	0.252	0.23	40.0	2.90	1.2	3.09	1063	8.3	8.3	<5
74	0.252	0.23	30.0	2.90	1.2	2.63	1044	7.1	6.6	−7
75	0.252	0.23	25.0	2.90	1.2	2.42	1002	6.5	5.5	−16
76	0.252	0.23	20.0	2.90	1.2	1.24	955	4.7	4.3	−8
77	0.252	0.23	18.0	2.90	1.2	1.78	913	4.8	3.6	−25
78	0.252	0.33	90.5	2.02	1.7	8.60		23.2	24.3	<5
79	0.252	0.33	80.0	2.02	1.7	8.45		22.8	23.8	<5
80	0.252	0.33	60.0	2.02	1.7	7.65		20.6	21.8	+6

Table A6. Composition and performance of cotton strands of Moussa (1976) at different ambient pressures and oxygen fractions, $d = 8.6\ mm$, $\rho_f = 60\ kg/m^3$, $f_b = 0.96$, $f_w = 0.04$ and $f_{ash} = 0.02$.

No.	f_{eff}	Y_{ox}	p_a kPa	S	B	$\dot{r}$ mm/min	T_s Exp, K	T_s Exp, K	Re_r	Re Corlin
100	0.288	0.21	101	3.63	1.3	9.1		1107	6.5	11.1
101	0.288	0.27	100	2.87	1.6	14.3		1158	10.2	18.7
102	0.288	0.21	102	3.28	1.4	7.9		1122	7.7	11.5
110	0.288	0.15	188	4.99	0.9	7.3	950	1128	5.2	5.5
111	0.288	0.23	102	3.28	1.4	12.7	965	1128	9.1	14.3
112	0.288	0.21	188	3.70	1.2	12.3	985	1170	8.8	13.9
120	0.288	0.23	245	3.28	1.3	18.0		1190	12.9	19.4
121	0.288	0.17	129	4.26	1.3	6.9		1190	4.9	7.1
122	0.288	0.20	115	3.81	1.2	9.9		1106	7.3	10.3
126	0.288	0.16	132	3.81	1.2	Ext	880	1106	Ext	Ext

Table A7. Composition and performance of incense sticks of Lin, Chow, and Huang (2021) at different ambient pressures and oxygen fractions, $p_a = 101\ kPa$, $\rho_f = 970\ kg/m^3$, $f_b = 0.86$ (50–52) and 0.84 (53–55), $f_w = 0.05$ and $f_{ash} = 0.11$.

No.	f_{eff}	d mm	ρ_f kg/m³	S	B	$\dot{r}$ mm/min	h/d	Re_r Exp	Re Corlin	Error %
50	0.258	5.0	720	2.9	1.2	3.03	1.6	15.2	12.0	−20
51	0.258	2.5	720	2.9	1.2	4.74	1.5	11.9	10.9	−8
52	0.258	1.5	720	2.9	1.2	7.17	1.3	10.8	10.4	<5
53	0.252	1.5	720	2.9	1.2	7.20		10.8	10.4	<5
54	0.252	1.5	920	2.9	1.2	5.7		10.9	10.4	<5
55	0.252	1.5	1100	2.9	1.2	4.3		9.9	10.4	5

Table A8. Composition and performance of char cones at different diameters of Yan et al. (2022).

No.	f_{eff}	d mm	ρ_f kg/m³	S	B	$\dot{r}$ mm/min	h/d	Re_r Exp	Re Corlin	Error %
56	0.71	2.27	444	7.7	3.3	11.1	3.96	15.5	14.3	<5
57	0.71	3.80	444	7.7	3.3	7.8	4.16	18.3	16.1	−12
58	0.71	6.30	444	7.7	3.3	6.8	5.05	26.4	19.1	−28
59	0.45	2.10	674	5.2	2.2	3.1	1.31	6.0	12.1	+102
60	0.45	3.50	674	5.2	2.2	2.5	1.85	8.0	13.3	+66
61	0.45	6.00	674	5.2	2.2	2.5	2.01	13.8	15.2	+10